Modeling of SrTiO3 polycrystalline substrate grain growth for tuning thin film functional properties

Marie Dallocchio, Charles Manière, Jérôme Lecourt, Ulrike Lüders, Wilfrid Prellier, Adrian David, Arnaud Fouchet

Modeling of $SrTiO_3$ polycrystalline substrate grain growth for tuning thin film functional properties.

Marie Dallocchio[1], Charles Manière[1*], Jérôme Lecourt[1], Ulrike Lüders[1], Wilfrid Prellier[1], Adrian David[1], Arnaud Fouchet[1*].
[1] NORMANDIE UNIV, ENSICAEN, UNICAEN, CNRS, CRISMAT, 14000 CAEN, FRANCE.

* Corresponding authors:
E-mail: arnaud.fouchet@ensicaen.fr; charles.maniere@ensicaen.fr

Abstract:
In the Combinatorial Substrate Epitaxy (CSE) approach, a thin film is grown at high temperature on a polycrystalline substrate. Those substrates induce a local film epitaxy on each substrate grain and an overall polycrystalline character on the macroscopic scale. Compared to single-crystalline films, this approach provides the possibility to introduce, in a controlled way, grain boundaries providing new functionalities. Therefore, controlling the microstructure and grain size of the substrates is an important step for tuning the film properties. In this paper, a complete study of the granular growth of the standard substrate material for the deposition of perovskite thin films, $SrTiO_3$, has been carried out with different isothermal cycles highlighting the grain growth mechanisms. From these results, we are able to predict the sintering thermal cycle necessary for targeting very precisely a desired grain size and the corresponding physical properties. Indeed, highly restraint physical properties specifications are needed for advanced electronic applications. Since a classic granular growth model was used, this approach can be generalized to the broad family of oxides.

Graphical Abstract

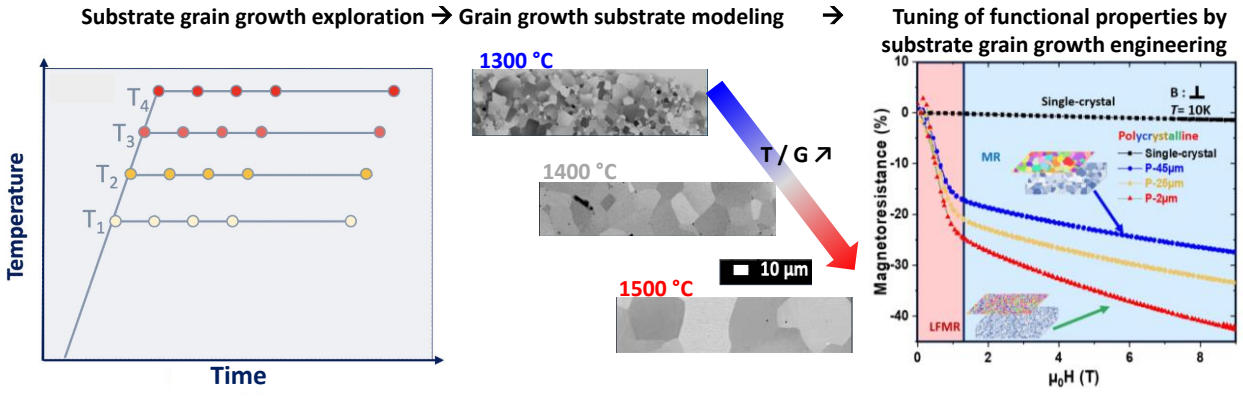

Keywords: Modeling, Polycrystalline substrates, Grain growth, Functional thin film.

Nomenclature:

G Grain size (m)
G_f Fit of experimental grain size (m)
$\dot{G}$ Grain growth rate ($m.s^{-1}$)
t time (s)
a, b, c fitting constants (c, between 0 and 1)
K(T) Diffusional factor ($m^{1+p}.s^{-1}$)
K_0 Grain growth pre-exponential factor ($m^{1+p}.s^{-1}$)
R Gas constant (8.314) ($J.mol^{-1}.K^{-1}$)
T Temperature (K)
K' Diffusional factor for isothermal conditions($m^{1+p}.s^{-1}$)
p Grain growth exponent
Q Grain growth activation energy ($J.mol^{-1}$)

1. Introduction

The Combinatorial Substrate Epitaxy (CSE) approach is based on growth of thin films upon polycrystalline substrates, which present grains of all possible crystalline orientations and was primarily used for the investigation of epitaxial relationships between complex oxides grown on a polycrystalline substrate. This film orientation library can indeed be achieved on one single sample and therefore studied with a unique deposition instead of numerous separated experiments on commercial single-crystalline substrates. This method was first focused on understanding the growth of non-isostructural film-substrate pairs [1,2], then on investigating complex oxide multilayer films exhibiting functional properties [3] and for the investigation of nanostructures epitaxially grown on perovskite films [4].

The cost of these substrates is much lower compared to the widely used single-crystal substrates, which need expensive and slow growth techniques, since standard and fast ceramic synthesis techniques are used. Such an approach is useful to develop the growth of complex oxides on low-cost, ceramic substrates, with a possibility of up-scaling of the production, as the principal limit is the size of the crucible during the substrate sintering. The substrates used for this technique are mirror polished disks of ceramic pellets, sintered by spark plasma sintering (SPS). Furthermore, such substrates have the advantage of being adapted to a wide range of functional oxides.

Several kinds of substrates were already been developed including exotic phases, such as layered perovskite $La_2Ti_2O_7$, as substrate to promote the growth of pyrochlore phase [5]; or the growth of Ruddlesden–Popper (RP) phase on isostructural substrates [6]. More common phases were also investigated such as rhombohedral Al_2O_3 [7], perovskite $LaAlO_3$ (LAO) [3] and the standard substrate $SrTiO_3$ (STO) [8], which was shown to have an atomically flat surface at the local scale.

Since the anisotropies of the functional properties of complex oxides (magnetism, ferroelectricity, etc.) are typically related to their crystalline orientation, different studies have been carried out in order to study their properties depending on the local grain orientation [3].

More recently, another degree of freedom of those substrates was explored with the control of the grain metrics as it can be used as a new tuning factor for functional properties. This is particularly true for thermoelectric properties in $SrRuO_3$ thin films, where the long-range translational symmetry breaking modifies the properties compared to single-crystal films [9], or for magneto-

resistive properties in $La_{0.7}Sr_{0.3}MnO_3$ thin films with different domain grain sizes from 2 μm to 45 μm [10].

In this context, we have studied the STO perovskite substrate granular growth with different isothermal cycles. By using a granular growth model, we are now able to predict the SPS parameters in order to obtain the expected grain size.

Although the effect of the grain metrics on the properties of the thin films has therefore been studied, the preparation of a substrate with the optimal grain metrics adapted to the thin film material is still done by trial and error. However, classic granular growth models are well suited to predict SPS sintered ceramics microstructure development [11] and therefore to the polycrystalline CSE substrates. In this study, we will show an example on the standard substrate STO being used for the deposition of a large number of different perovskite oxide thin films and therefore of an outstanding importance for the field. The description of the grain metrics obtained by different isothermal sintering cycles by a granular growth model is extended to predict the grain size under specific conditions, and can be therefore used to determine the sintering conditions to obtain the grain metrics being optimal for the chosen thin film material and its properties. This methodology can be generalized to many other oxides, providing therefore a handle to optimize grain metrics for a general CSE approach avoiding time consuming trial and error studies.

2. Material and methods

All STO ceramics were synthetized starting from the two precursors TiO_2 and $SrCO_3$ [10]. These precursors were calcined for 12 hours at 1200 °C. Then, to eliminate the agglomerates, these calcined powders were ground mechanically for 16 min before sintering by SPS. Once the STO powder is obtained, 4 g is introduced into a 20 mm diameter mold covered with a graphite foil (Papyex®). For the SPS, different dwell temperatures (i.e. 1200 °C, 1300 °C, 1400 °C and 1500 °C) were studied with heating/cooling ramps of 100 °C/min. A pressure of 22 MPa is applied during the heating and cooling. During the isothermal stage, the pressure is increased to 51 MPa to ensure full densification. All SPS syntheses were carried out at 0.04 hPa. In order to identify the grain growth behavior, different dwelling times were explored: 0 min, 5 min, 10 min, 20 min or 60 min. Finally, a 2 cm diameter pellet is obtained.

Afterwards, the sintered pellets are cut and polished to obtain flat surfaces. The polishing process is started by manual polishing using several SiC papers decreasing successively the grain size and finishes with automatic steps using a Struers polisher with diamond liquid pastes (3 μm and 1 μm). Finally, the samples are polished with a Si-colloidal solution, in order to obtain a mirror-like surface [8]. The STO structural analysis were characterized by XRD and show that STO phase is more than 99% pure, and 1% impurities are attributed to different strontium or titanium oxides. The microstructures and relative densities were analyzed by SEM using the Jeol 7200 LV scanning electron microscope and measured by Archimedes' method, respectively. Only planar substrate surfaces were analyzed because it is the substrate surface that influence the deposited layer structuration.

The mean grain size was measured using the linear intercept method. The measurement was performed with at least 6 lines each intercepting at least 10 grains for each image and on different images. Different images are used of each sample to calculate the average grain size. Then a correction factor of 1.56 was used as described by Mendelson [12] to transform the 1D average grain size into a stereological determination of the average 3D grain size.

$La_{0.67}Sr_{0.33}MnO_3$ (LSMO) thin films of 40 nm have been grown by pulsed laser deposition (PLD). The depositions were carried out at 645 °C under oxygen-ozone mixture conditions, with a partial pressure of $6.4x10^{-4}$ mbar. A KrF excimer laser (λ= 248 nm) was used with a repetition rate of 2 Hz and a deposition rate close to 0.1 Å per laser pulse [13].
The simulation of the grain growth curves has been done by the Octave forge software. A script has been constructed to simulate the ordinary differential equations of grain growth detailed in the following. The script allows to simulate all the sintering thermal cycle.

3. Theory/calculations

Most grain growth laws are controlled by the diffusion of chemical species from grain to grain. The granular growth rate is then defined by equation 1 and 2 [14]:

$$\dot{G} = \frac{\mathrm{K(T)}}{G^p} \qquad \text{Equation 1}$$

With K(T) which can be expressed by an Arrhenius law:

$$\mathrm{K(T)} = K_0 exp(\frac{-\mathrm{Q}}{RT}) \qquad \text{Equation 2}$$

This relation is generally transcribed in its integral form, for mechanisms analysis under isothermal conditions:

$$G^{p+1} = G_0^{p+1} + K't \qquad \text{Equation 3}$$

In this new form, the exponent p+1 can be related to specific grain growth mechanisms [14], typically p+1= 4 for surface diffusion and p+1= 3 for lattice diffusion.

Thereby, the different steps to obtain grain growth parameters using the traditional grain growth model identification method are defined below and summarized in figure 1a to d:

a. Experimental exploration: The first step consists in collecting the experimental data and highlighting the grain sizes according to the different temperatures and dwell times. These data will allow us to obtain isothermal growth curves at the four temperatures studied: 1200 °C, 1300 °C, 1400 °C and 1500 °C with different holding times of 0 min, 5 min, 10 min, 20 min and 60 min.

b. Determination of the isothermal grain growth rate curve: For the second step, a mathematical fit of the experimental data will be used to determine the grain growth rate. The equation used for this fit is:

$$G_f = \mathrm{a} + \mathrm{b}t^c \qquad \text{Equation 4}$$

With c between 0 and 1.

c. Determination of grain growth model isothermal constants: The third step aims at determining p and K (T) *via* a linear regression for each of our temperatures. To do this, equation 1 is taken in its logarithmic form:

$$\ln(\dot{G}) = \ln(\mathrm{K(T)}) - p\ln(G) \qquad \text{Equation 5}$$

d. Determination of K(T) thermal dependence: Finally, the last step is the identification of the activation energy (Q) and the pre-exponential constant (K_0). For this, a second linear regression from equation 2 is conducted. The regression equation is :

$$\ln(\mathrm{K(T)}) = \ln K_0 - \frac{\mathrm{Q}}{RT} \qquad \text{Equation 6}$$

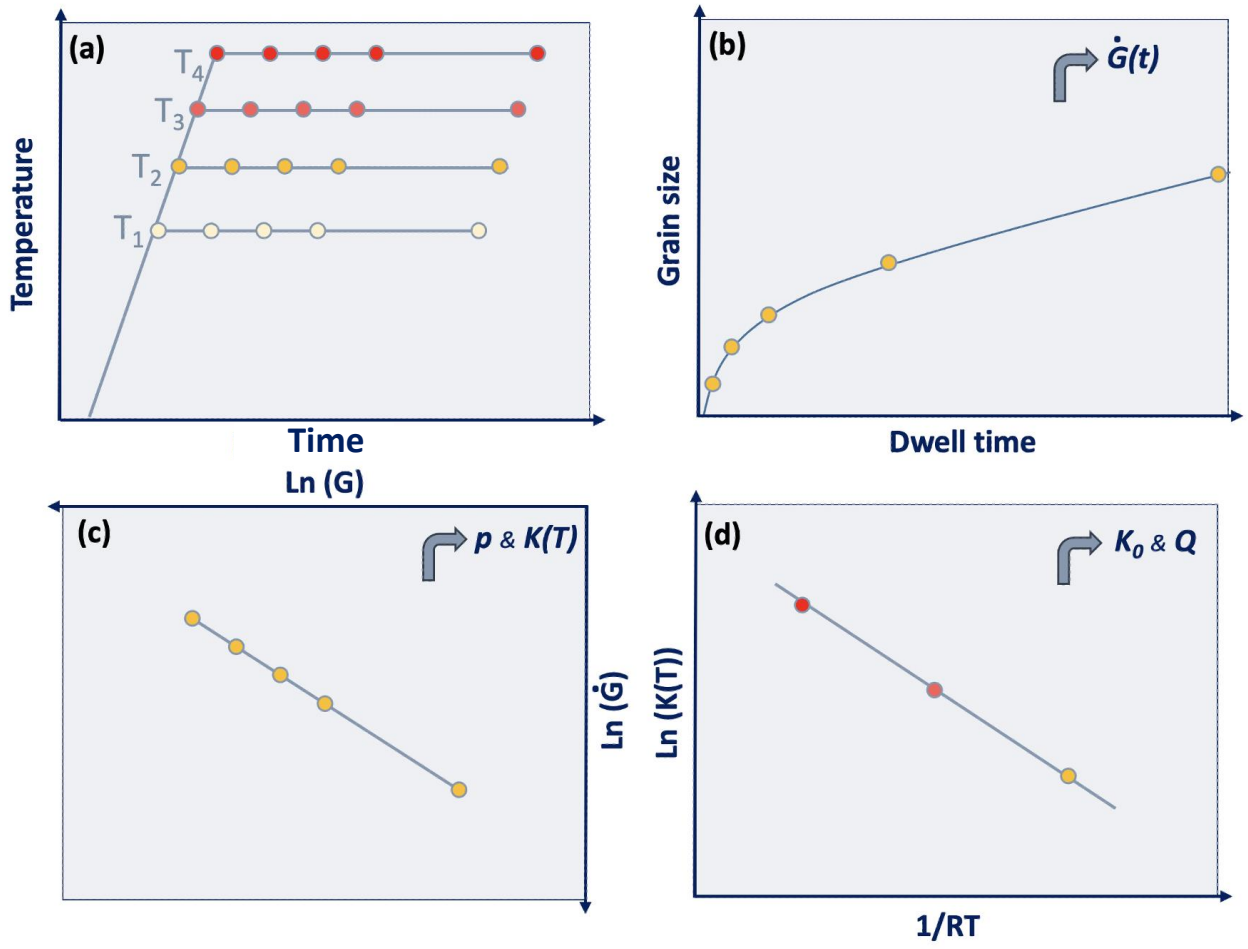

Figure 1. Steps of the grain growth model identification method including a) Experimental exploration, b) fitting and determination of the isothermal grain growth rate curve, c) determination of grain growth model isothermal constants, d) determination of the thermal dependence parameters K_0 and Q.

4. Results and discussion

4.A. Experimental exploration

In this section, we study each micrograph summarized in figure 2 and extract the average grain sizes and their standard deviations. This figure shows that all the microstructures have a nearly fully dense microstructures with only residual porosity. This justifies the use of SPS against conventional sintering that would result in higher porosity for the lower temperatures. SPS offers the opportunity to test different substrate grain sizes without porosity disturbances.

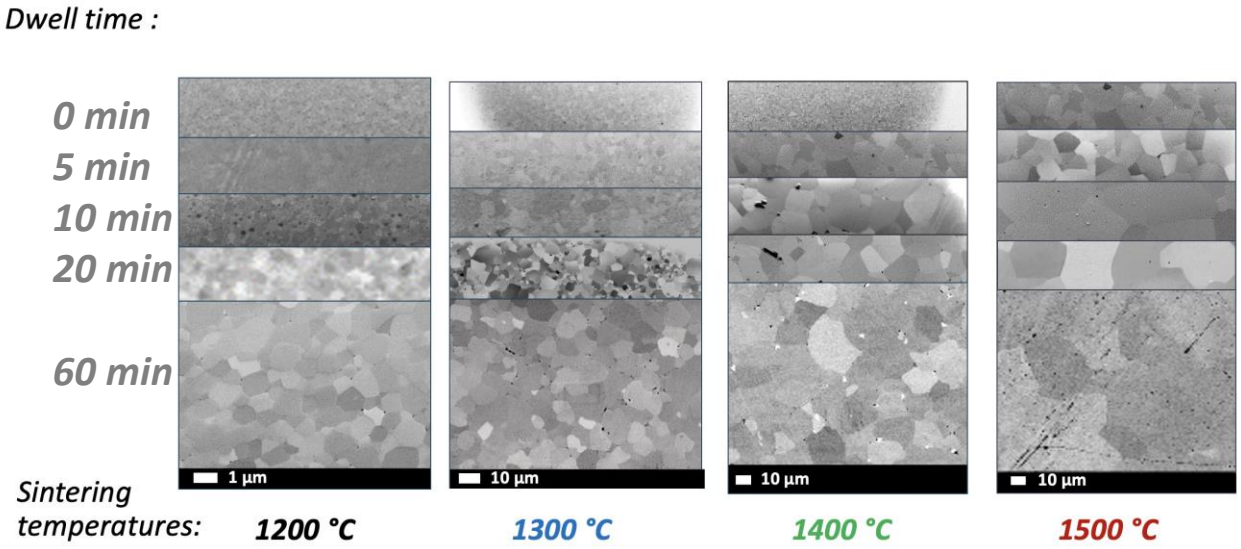

Figure 2. *SEM images used to determine grain size.*

Table 1 presents all identified average grain sizes corresponding to the temperature and dwell times. We can see the high dependency of the grain growth kinetics with the sintering temperature by the very slow grain growth rate for 1200 °C and a significant grain growth rate above 1300 °C. For 1200 °C, the grain growth is too slow to obtain a clear quantification of the grain size with the used dwelling times, so that this temperature is removed from the identification process.

Table 1. *Summary of average grain diameters and their standard deviation for each sample.*

Temperature (°C) \ Dwell time (min)	0	5	10	20	60	
1200	1.310 0.468	1.794 0.510	2.028 0.595	2.172 0.637	1.445 0.515	Grains size σ, standard deviation (µm)
1300	3.120 1.203	4.267 2.301	4.533 2.655	6.427 3.865	9.207 3.508	
1400	1.948 2.145	12.615 5.223	19.968 7.680	22.859 10.746	30.046 11.178	
1500	10.964 6.743	24.371 7.841	32.852 12.361	40.432 14.413	62.447 30.103	

4.B. Fitting and determination of isothermal grain growth rate curve

Figure 3 represents the evolution of experimental average grain sizes with dwell times for the different temperatures. As already observed in the micrographs, the grain growth for the lowest sintering temperatures (1200 and 1300 °C) remains quite low. For each isothermal dwell, the trend has a classic logarithmic form of the granular growth with a very high speed at the beginning and a progressive attenuation with time. This is why we have explored many dwelling times in the region where the grain size variation is strong. As predicted by the model, grain growth rates increase strongly with the sintering temperature.

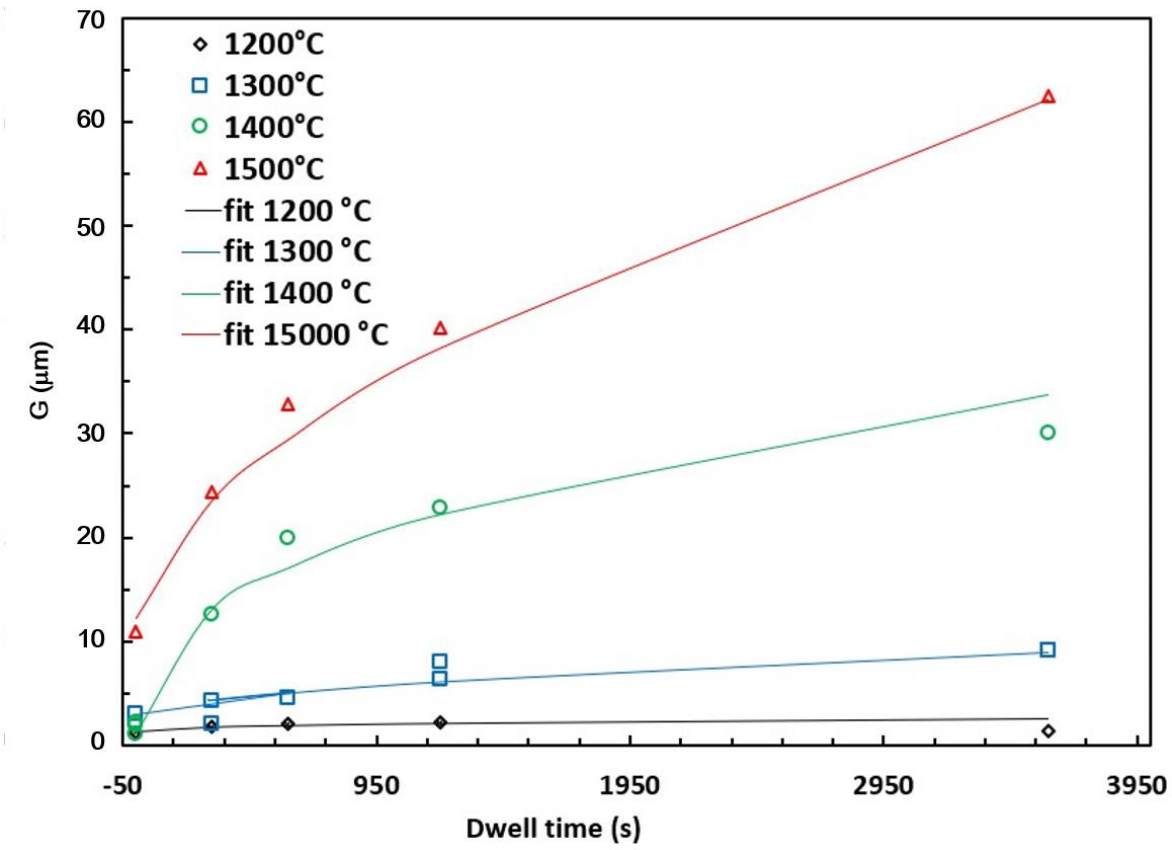

Figure 3*. Grain sizes vs dwell time and mathematically fitted grain growth curves.*

The grain growth curves were then mathematically fitted using equation 4 (see figure 3 continuous lines). From these curves, the grain growth rates were easily calculated taking the time derivative of equation (4) for each dwelling time. We can then proceed to the next step with the determination of the grain growth exponent (p) and the pre-exponential factor (K).

4.C. Determination of grain growth model isothermal constants

Figure 4 shows the logarithm of grain growth rate $\dot{G}$ as a function of the logarithm of grain size, G (see equation 3). Thus, the linear regression of each isotherm was calculated to extract several parameters: the slope gives the growth exponent ($-p$) and the origin gives pre-exponential factor (ln(K)). For a robust modeling, the factor p must be common for all isotherms (except for significant changes in the grain growth mechanism). The p values are included between $1.4 < p < 2.1$, which results in an average p of 1.728. Thanks to this fixed factor, we can deduce the growth exponent (K(T)) for each tested temperature. Thus, the isothermal constants of the model are: p = 1.73 and K(1300 °C) = 40.9; K(1400 °C)=37.5; K(1500 °C) = 35.6 $m^{1+p}.s^{-1}$.

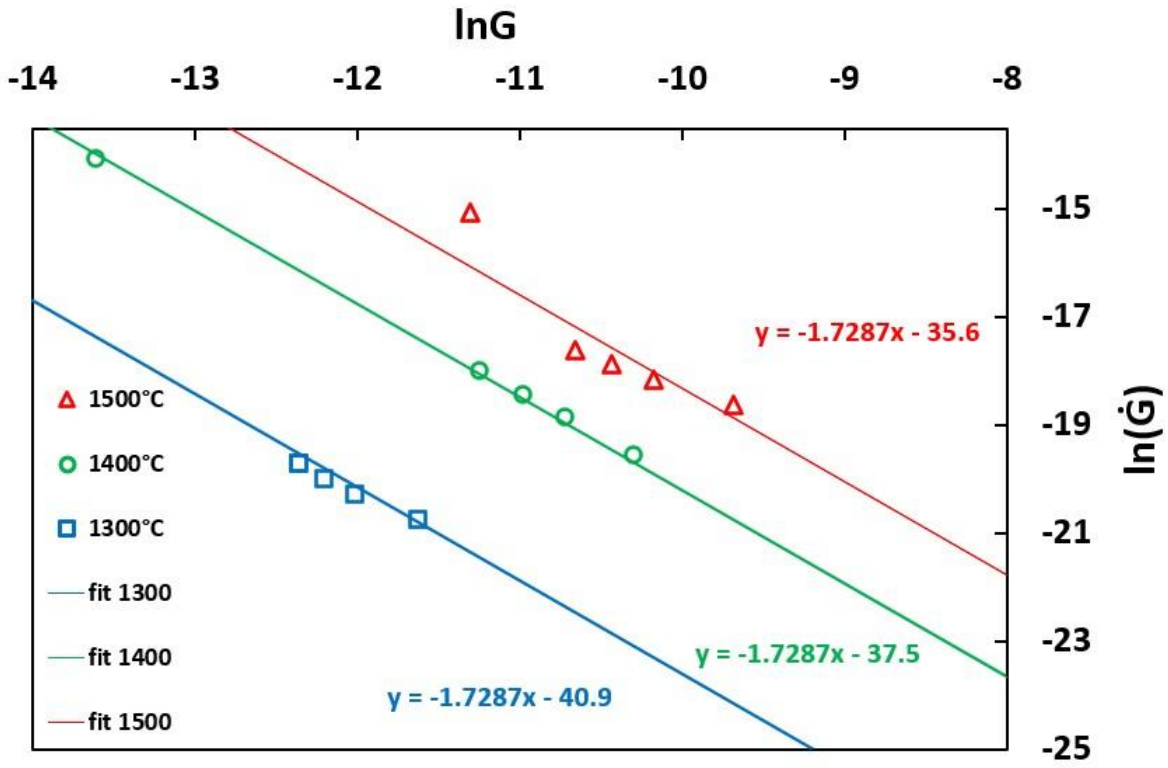

Figure 4. *Logarithm of the grain growth rate as a function of the logarithm of the grain size with the linear regression at each isotherm.*

Figure 4 was used to extract the parameters from equation 1 for each isotherm. Interpreting the growth exponent *p*, the mechanisms of diffusion in STO can be highlighted. In this case, a factor $p = 1.73$ is observed, close to 2, which according to equation 3 (typically use for isothermal cases) leads to a factor $p+1$ close to 3. An exponent $p+1 = 3$ is found for classic grain growth models [15]. Thus, according to the tables of Rahaman [14], this exponent of 3 refers to several mechanisms related to diffusional growth where the most probable is lattice diffusion.

4.D. Determination of the K parameter thermal dependence.

The last step before modeling the system is to calculate the diffusional terms (K_0) and the activation energy (Q) of the grain growth. The second regression equation (6) is thus plotted in figure 5 *vs* 1/RT, using the K values identified previously. The activation energy Q is determined by the slope and the K_0 term by the origin ($ln(K_0)$). The parameters extracted from our model are then $K_0 = 648$ $m^{p+1}.s^{-1}$ for the pre-exponential factor and $Q = 617$ $kJ.mol^{-1}$ for the activation energy. In conventional sintering, close value of activation energy were found with 724 kJ/mol [16] even if highly bimodal (abnormal) grain growth makes growth transition regime behaviors. SPS grain growth seems more stable, with classic behavior and do not shows abrupt regime transition.

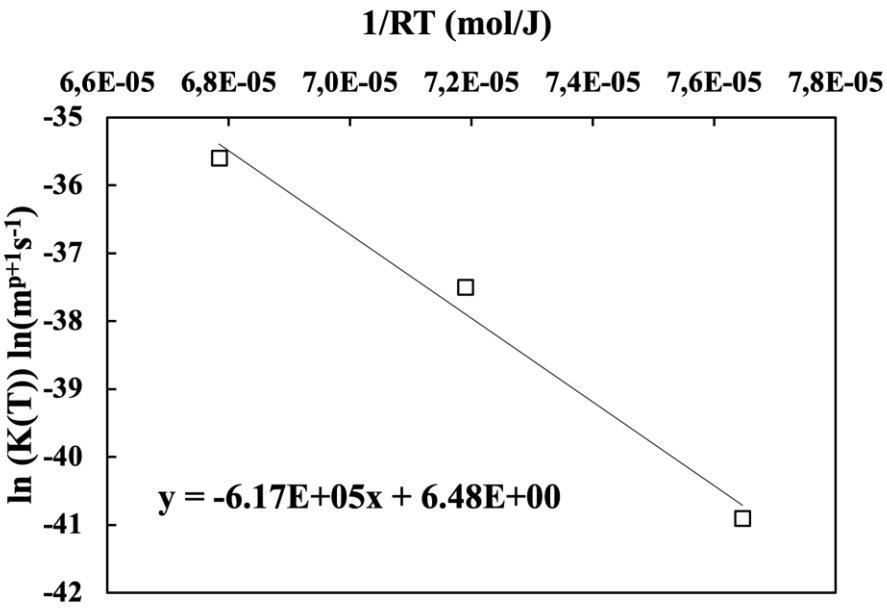

Figure 5. *Determination of the activation energy of grain growth using a traditional model.*

4.E. Grain Growth Modeling

By injecting these values into equations (1) and (2), the grain growth can thus be simulated using the typical grain growth model, easily determined by calculation of an ordinary differential equation problem on a software like Octave forge. The identified values of Q, K_0, p are introduced within the analytic model for each thermal cycle which simulates both heating and subsequent dwelling temperatures.

Thus, a direct comparison is possible between the experimental data and the theoretical results of this simulation (see figure 6). Even though the simulated values differ slightly from the experimental values (especially for higher temperatures), they still remain within the grain size distribution bar and gives a good prediction of the average grain sizes. This bar represents the standard deviation around the mean grain size value observed in the different SEM images. Although excluded from the analysis to obtain this model, the data from the samples sintered at 1200 °C compare well with the slow kinetics of the simulation model.

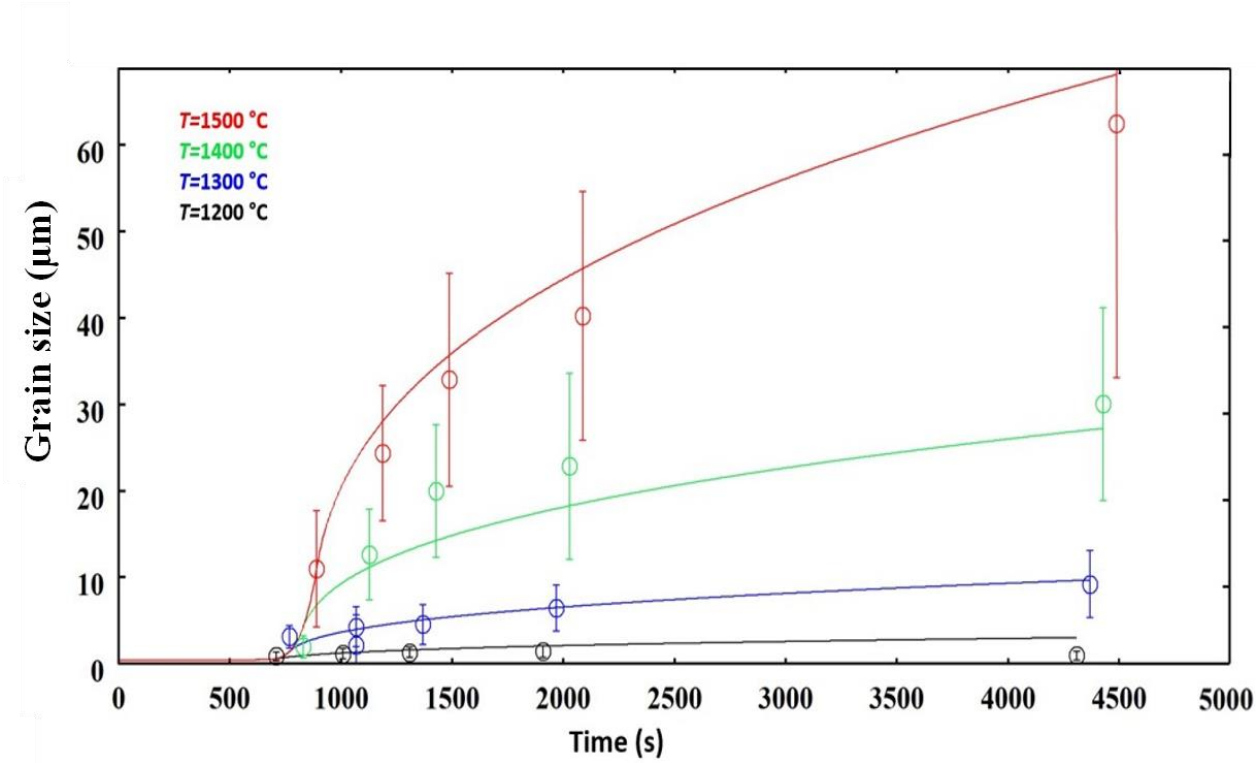

Figure 6*. Simulation of granular growth on polycrystalline STO substrates.*

4.F. Discussions

The grain metric is important for the introduction of grain boundaries and the tunability of the thin films functional properties. For example, those grain boundaries can bring extrinsic properties to the thin films such as in LSMO, which are not present for single crystal films (see figure 7) [10]. As we can see, at low temperature, single crystal films present a very small MR, whereas, the polycrystalline substrates induce new effect on the LSMO films with low field Magnetoresistance (LFMR), and an important MR. More importantly, those effects can be tuned by their density in the films as seen on figure 7, where this MR tends to increase with the decrease of the grain size and therefore the importance of the grain metric control of the polycrystalline substrates.

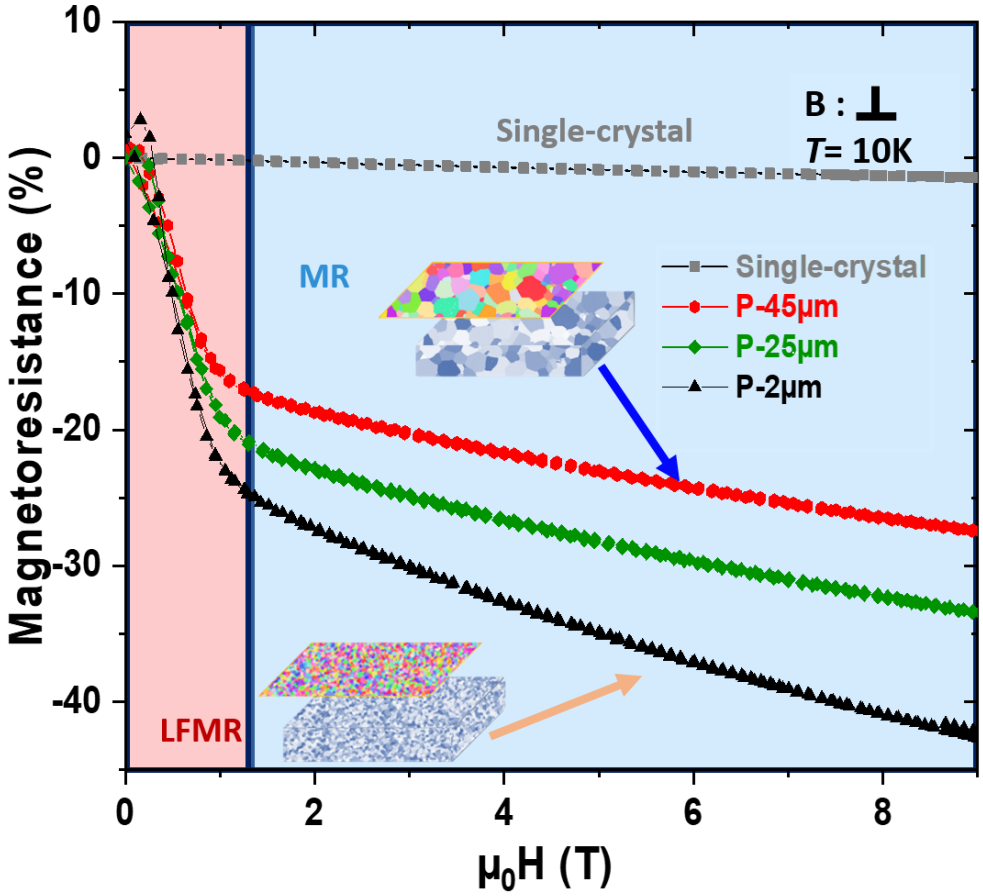

Figure 7*. Magnetoresistance obtained for LSMO films on polycrystalline STO substrate compare to single crystal substrate and their dependency with the different grain size (adapted from* [10]*).*

Another example is for thermoelectric properties, where the introduction of grain boundaries have also impacted the diffusion of mobile carriers [9] and an extensive study of the grain size effect can be of importance for tuning the properties on demand.

Finally, this approach realized on model system STO can be widen to other ceramic system based on perovskite materials and it will be interesting to test the granular growth model on those family of metal oxide. This provides also the possibility to locally induce strain effect [17] on the perovskite films and study relaxation effect with the grain metric. Furthermore, as the CSE approach is not limited to the perovskites materials, our study can also be extended to a broad family of metal oxide inducing pyrochlore, RP, etc.

In perspective, since our study is focused on grain size, CSE approach open also new perspectives with the studies of grain boundaries and their effects on the film growth and their interfacial properties. A complementary study can also be done related to texturation of the ceramics and his influence on the growth of thin films, which will be investigated in the future.

5. Conclusions

Controlling the grain size of polycrystalline substrates is a key aspect allowing to tune the properties of thin films deposited on top, as shown for instance for magnetotransport or thermoelectric properties. In this study, the grain growth behavior of STO substrates sintered by spark plasma sintering has been identified experimentally. The dominant grain growth mechanism is lattice diffusion. The use of spark plasma sintering allows to obtain well densified substrates were the grain sizes is less sensitive to abnormal grain growth and can be easily tuned from submicronic to nearly 100 μm. The grain growth kinetics were identified and modeled analytically. The model predicts well all experimental points in heating and dwelling regimes. Such model will be a precious tool to define experimental cycles allowing to attain different targeted substrates grains sizes corresponding to specific properties to be tuned.

Appendix

The initial powder has an average grain size of 0.444 μm. The SEM image and grain size distribution of the starting powder is reported in figure A. This shows the grain sizes are distributed from 0.1 to 1.4 μm. The grains have a coarse size which may explain a less responsive grain growth with apparent absence of abnormal grain growth that is often observed for STO[16].

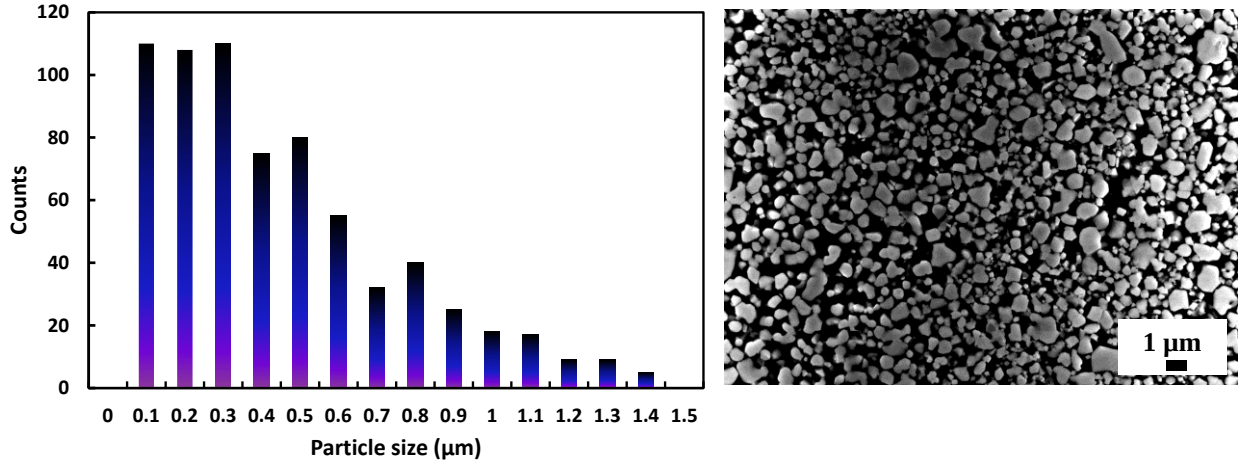

Figure A *Histogram of initial powder grain size distribution and SEM image of initial grains.*

Acknowledgements

The authors thank regional funding and french agence nationale de la recherche (ANR) (ANR-17-CE08-0012) in the framework of the POLYNASH project.

AUTHOR CONTRIBUTIONS

Arnaud Fouchet performed conceptualization, project administration, resources and writing– review & editing. Marie Dallocchio performed investigations, formal analysis, writing original draft. Charles Manière performed Data curation, conceptualization and writing – review and

editing. Jérôme Lecourt, Ulrike Lüders, Wilfrid Prellier, Adrian David performed Data curation, Formal analysis and writing – review and editing.

References

[1] N.V. Burbure, P.A. Salvador, G.S. Rohrer, Orientation and Phase Relationships between Titania Films and Polycrystalline BaTiO3 Substrates as Determined by Electron Backscatter Diffraction Mapping, Journal of the American Ceramic Society. 93 (2010) 2530–2533. https://doi.org/10.1111/j.1551-2916.2010.03878.x.

[2] N.V. Burbure, P.A. Salvador, G.S. Rohrer, Photochemical Reactivity of Titania Films on BaTiO3 Substrates: Influence of Titania Phase and Orientation, Chem. Mater. 22 (2010) 5831–5837. https://doi.org/10.1021/cm1018019.

[3] D. Pravarthana, M. Trassin, J. Haw Chu, M. Lacotte, A. David, R. Ramesh, P.A. Salvador, W. Prellier, BiFeO3/La0.7Sr0.3MnO3 heterostructures deposited on spark plasma sintered LaAlO3 substrates, Appl. Phys. Lett. 104 (2014) 082914. https://doi.org/10.1063/1.4867021.

[4] B. Bérini, M. Dallocchio, A. David, U. Lüders, Y. Bourlier, L. Rault, R. Coq Germanicus, W. Prellier, Y. Dumont, V. Demange, A. Fouchet, Morphology control of self-organised Sr3V2O8 nanostructures on SrVO3 grown onto single and poly-crystalline subjacent SrTiO3 substrates, Applied Surface Science. 566 (2021) 150759. https://doi.org/10.1016/j.apsusc.2021.150759.

[5] D. Pravarthana, O.I. Lebedev, A. David, A. Fouchet, M. Trassin, G.S. Rohrer, P.A. Salvador, W. Prellier, Metastable monoclinic [110] layered perovskite Dy $_2$ Ti $_2$ O $_7$ thin films for ferroelectric applications, RSC Adv. 9 (2019) 19895–19904. https://doi.org/10.1039/C9RA04554F.

[6] M. Lacotte, A. David, G.S. Rohrer, P.A. Salvador, W. Prellier, Preferential orientation relationships in Ca2MnO4 Ruddlesden-Popper thin films, Journal of Applied Physics. 118 (2015) 045306. https://doi.org/10.1063/1.4927518.

[7] D. Pravarthana, D. Chateigner, L. Lutterotti, M. Lacotte, S. Marinel, P.A. Dubos, I. Hervas, E. Hug, P.A. Salvador, W. Prellier, Growth and texture of spark plasma sintered Al $_2$\$ O $_3$\$ ceramics: A combined analysis of X-rays and electron back scatter diffraction, Journal of Applied Physics. 113 (2013) 153510. https://doi.org/10.1063/1.4802439.

[8] S. Woo, H. Jeong, S.A. Lee, H. Seo, M. Lacotte, A. David, H.Y. Kim, W. Prellier, Y. Kim, W.S. Choi, Surface properties of atomically flat poly-crystalline SrTiO3, Sci Rep. 5 (2015) 8822. https://doi.org/10.1038/srep08822.

[9] S. Woo, S.A. Lee, H. Mun, Y.G. Choi, C.J. Zhung, S. Shin, M. Lacotte, A. David, W. Prellier, T. Park, W.N. Kang, J.S. Lee, S.W. Kim, W.S. Choi, Enhanced magnetic and thermoelectric properties in epitaxial polycrystalline SrRuO3 thin films, Nanoscale. 10 (2018) 4377–4384. https://doi.org/10.1039/C7NR09627E.

[10] M. Dallocchio, A. Boileau, B. Mercey, A. David, U. Lüders, S. Froissart, X. Larose, B. Bérini, Y. Dumont, A. Pautrat, W. Prellier, A. Fouchet, Tunable magnetic and magnetotransport properties in locally epitaxial La 0.67 Sr 0.33 MnO 3 thin films on polycrystalline SrTiO 3 , by control of grain size, Journal of Physics D: Applied Physics. 55 (2022) 1–11. https://doi.org/10.1088/1361-6463/ac5a1f.

[11] C. Manière, L. Durand, A. Weibel, C. Estournès, A predictive model to reflect the final stage of spark plasma sintering of submicronic α-alumina, Ceramics International. 42 (2016) 9274–9277. https://doi.org/10.1016/j.ceramint.2016.02.048.
[12] M.I. Mendelson, Average Grain Size in Polycrystalline Ceramics, J American Ceramic Society. 52 (1969) 443–446. https://doi.org/10.1111/j.1151-2916.1969.tb11975.x.
[13] A. Boileau, M. Dallocchio, F. Baudouin, A. David, U. Lüders, B. Mercey, A. Pautrat, V. Demange, M. Guilloux-Viry, W. Prellier, A. Fouchet, Textured Manganite Films Anywhere, ACS Appl. Mater. Interfaces. 11 (2019) 37302–37312. https://doi.org/10.1021/acsami.9b12209.
[14] Sintering of Ceramics | Mohamed N. Rahaman | Taylor & Francis Group, (2021). https://www.taylorfrancis.com/books/mono/10.1201/b15869/sintering-ceramics-mohamed-rahaman (accessed September 29, 2021).
[15] R.M. German, P. Suri, S.J. Park, Review: liquid phase sintering, J Mater Sci. 44 (2009) 1–39. https://doi.org/10.1007/s10853-008-3008-0.
[16] W. Rheinheimer, E. Schoof, M. Selzer, B. Nestler, M.J. Hoffmann, Non-Arrhenius grain growth in strontium titanate: Quantification of bimodal grain growth, Acta Materialia. 174 (2019) 105–115. https://doi.org/10.1016/j.actamat.2019.05.040.
[17] D.G. Schlom, L.-Q. Chen, C.J. Fennie, V. Gopalan, D.A. Muller, X. Pan, R. Ramesh, R. Uecker, Elastic strain engineering of ferroic oxides, MRS Bulletin. 39 (2014) 118–130. https://doi.org/10.1557/mrs.2014.1.